2019 International Conference on Robotics and Automation (ICRA)
Palais des congres de Montreal, Montreal, Canada, May 20-24, 2019

Design and Analysis of A Miniature Two-Wheg Climbing Robot with Robust Internal and External Transitioning Capabilities

Darren C. Y. Koh[1,*], Audelia G. Dharmawan[1,*], Hassan H. Hariri[1,2], Gim Song Soh[1], Shaohui Foong[1], Roland Bouffanais[1], Hong Yee Low[1], and Kristin L. Wood[1]

***Abstract*— Plane-to-plane transitioning has been a significant challenge for climbing robots. To accomplish this, additional actuator or robot module is usually required which significantly increases both size and weight of the robot. This paper presents a two-wheg miniature climbing robot with a novel passive vertical tail component which results in robust transitioning capabilities. The design decision was derived from an in-depth force analysis of the climbing robot while performing the transition. The theoretical analysis is verified through a working prototype with robust transitioning capabilities whose performance follows closely the analytical prediction. The climbing robot is able to climb any slope angles, 4-way internal transitions, and 4-way external transitions. This work contributes to the understanding and advancement of the transitioning capabilities and the design of a simple climbing robot, which expands the possibilities of scaling down miniature climbing robot further.**

I. INTRODUCTION

Climbing robots have many benefits such as a highly-expanded workspace and the ability to reach or accomplish otherwise impossible spots or tasks for ground robots. When climbing robots are used collaboratively with unmanned ground vehicles (UGV) for indoor autonomous intelligence, surveillance and reconnaissance (ISR) missions, they can be a powerful swarm that collectively completes tasks such as mapping, detection, monitoring and tracking. Specifically, the climbing robot can be used to provide an overall image of the area and as a bridge for communication for robots on different floors. To complete such tasks, the robot may be required to climb obstacles and transition from one plane to another, both internally (concave angle) and externally (convex angle).

Among the various attachment means, such as magnetic attachment [1], vacuum suction [2], gripping capability [3], and electro-adhesive technology [4], adhesive tapes have the advantages of being lightweight, operationally quiet, and energy efficient to be used in miniature robots [5]. Different types of robots can use adhesive tapes, such as track-based [6], legged [7], and wheel-leg (wheg) [8], [9]. It has been observed from nature that the mechanism for attachment to the surface in climbing animals is completely different from its detachment [10]. The general principle is found to be an entire-surface attachment and a peeling-like detachment such that strong adhesion is instantaneously generated while minimal effort is needed for contact release. For miniature robots, designing bulky legged mechanism to fulfil this is undesirable. While a track-based vehicle is unable to produce this locomotion, a more effective approach is to employ the wheg configuration with compliant adhesive to passively achieve the required motion.

Most of the existing miniature climbing robots are only capable of flat surface climbing, and either have no or limited internal plane-to-plane transition capabilities. Those that are capable of performing external transitions usually need additional active tail or body joint, as summarized in Table I, to support the robot while it transits to make contact with the adjacent surface before pulling the rest of its body. These then require additional actuators and/or body segments which increase the size and mass of the robot significantly.

The objective of this paper is to study and develop a two-wheg miniature climbing robot which can perform plane-to-plane transitioning robustly. As external transitions are the hardest to achieve based on the literature review, the requirements for successful external transitions are analyzed and discussed. The outcome of the analysis is a design basis to achieve a two-wheg miniature climbing robot with robust transitioning capabilities without requiring additional active actuator or body joint to keep the robot scaled-down.

II. THE CLIMBING ROBOT: ORION-III

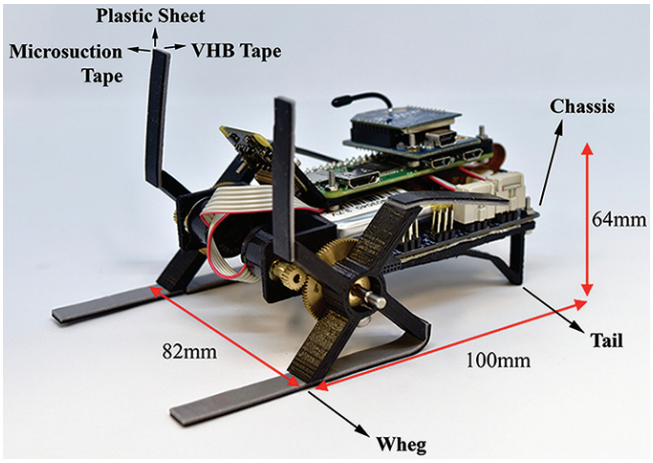

Fig. 1. The miniature two-wheg climbing robot with novel vertical tail component for robust transitioning capabilities. It weighs 137.5 g and is equipped with electronics for ISR task: microcontroller, IMU, Raspberry Pi Zero and camera module, and XBee communication module.

The authors gratefully acknowledge the support of TL@SUTD-Systems Technology for Autonomous Reconnaissance & Surveillance and SUTD-MIT International Design Center (http://idc.sutd.edu.sg)

*These authors contributed equally to this work

[1]Singapore University of Technology and Design, Engineering Product Development Pillar, Singapore sohgimsong@sutd.edu.sg

[2]Rafik Hariri University, Mechanical and Mechatronic Engineering, Lebanon

	Stickybot [11]	Waalbot [12]	Inverted Mini-Whegs [13]	Tankbot [14]	Seo et al. [15]	CMWB00 [16]	ORION-III
Int. trans.	No	2 ways	2 ways	2 ways	3 ways	4 ways	4 ways
Ext. trans.	No	No	No	1 way	2 ways	2 ways	4 ways
Method	None	Passive tail/ chassis	Passive tail/ chassis	Active tail	Passive body joint	Active body joint	Passive vertical tail

TABLE I
EXISTING MINIATURE CLIMBING ROBOTS AND ORION-III.

Shown in Fig. 1, the architecture of the developed climbing robot, ORION-III, can be categorised into three parts: whegs, chassis, tail. The chassis houses similar electronics required for ISR task as the previous version ORION-II [17], and two DC motors each driving a wheg with four "flaps" equipped with compliant adhesive tape. There is a 4:1 gear reduction between the motor and the whegs. The main difference between ORION-III and ORION-II is the additional novel vertical tail component that helps a lot in accomplishing robust external transitions based on the analysis which will be discussed in more detail later. The dimensions of the robot are 100 mm $\times$ 82 mm $\times$ 64 mm and the mass is 137.5 g.

The adhesive tape used in the climbing robot consists of three layers: a 0.8 mm AirStick^{TM} Microsuction tape by Sewell, a 0.18 mm plastic sheet, and a 3M VHB tape. The surface of a microsuction tape consists of thousands of microscopic air pockets which can create partial vacuums between the tape and the target surface. The thinness of the microsuction tape makes it very susceptible to deformation, and hence an additional flexible plastic sheet is added to help the compliant microsuction tape to return to its original flat shape to encourage maximum contact between the adhesive and surface. The unstructured backing layer of polymer (3M tape) of different elastic behaviour creates a gradient in the viscoelastic property, which has been shown to enhance the adhesive force of adhesive material [18].

A. Adhesive Characterization

The tri-layer adhesive used is characterized for its adhesion through measurement on a universal testing system. A 15 mm $\times$ 15 mm adhesive sample was loaded to an Instron Series 5982. A preload force ranging from 0.05 N to 300 N was applied with an acrylic plate before the normal peel-off measurement was conducted. Data recorded by the machine represents the normal adhesive force corresponding to the applied preload force. The preload and the normal adhesive force recorded are normalised over the adhesive area to give the preload pressure and the normal adhesive pressure respectively. The resulting performance of the adhesive used is shown in Fig. 2(a), with the fitted power law function $P_A = a\,{P_P}^{1/n}$, where P_A is the adhesion pressure, P_P is the preload pressure, a is a scaling coefficient, and $n > 1$, which is the common fitted function to characterize adhesive performance where the adhesion is greater than preload for low preload pressures and saturates to a maximum adhesion value at high preload pressures. These data will be useful to identify the adhesive requirements [19].

III. ROBOT MODELING & FORCE ANALYSIS

This section analyzes the failure and success conditions for external transitioning of a two-wheg climbing robot, in terms of the robot design criteria and the adhesive requirements.

A. External Transition Modeling

The two-wheg climbing robot is first modeled as a chain of linkages to obtain its configuration at different possible instances when transiting externally. Fig. 2(b) shows the mechanism model of the robot during the external transition (-90° convex angle between the first and second surface). The robot's adhesive pivot $\mathbf{P}$ can make contact with the second surface at different distance q from the intersecting corner $\mathbf{U}$ of the surfaces, with $q \leq r - J_d$, r is the wheg's radius and J_d is the distance between the wheg's shaft and the chassis.

It is observed that at the initial contact with the second surface, the robot's configuration is such that the chassis is in contact with the intersecting corner point $\mathbf{U}$ and the robot's tail point $\mathbf{B_e}$ is in contact with the first surface, as depicted in Fig. 2(b). Hence, the following coordinate transformations relative to the origin frame at point $\mathbf{O_e}$ can be obtained:

$$\begin{Bmatrix} \mathbf{U} \\ 1 \end{Bmatrix} = Z(\sigma)X(r)Z(\lambda+90^\circ)X(J_d)Z(-90^\circ)X(U_d)\begin{Bmatrix} 0 \\ 0 \\ 1 \end{Bmatrix}$$
$$= \begin{Bmatrix} r\cos\sigma + U_d\cos(\sigma+\lambda) - J_d\sin(\sigma+\lambda) \\ r\sin\sigma + U_d\sin(\sigma+\lambda) + J_d\cos(\sigma+\lambda) \\ 1 \end{Bmatrix} \equiv \begin{Bmatrix} q \\ e \\ 1 \end{Bmatrix} \quad (1)$$

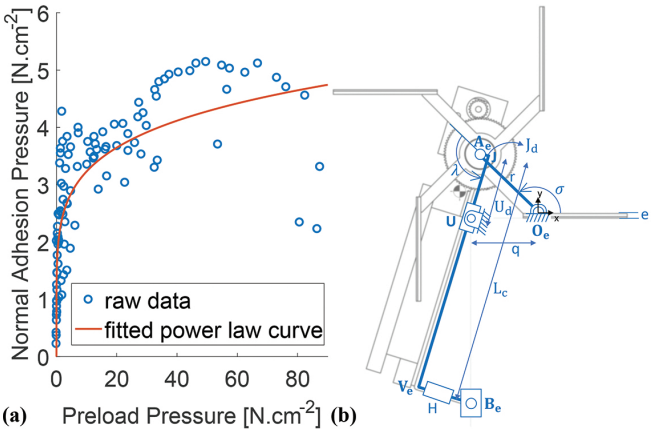

Fig. 2. (a) Performance curve of the adhesive on an acrylic surface, and (b) Mechanism model for the climbing robot's configuration.

$$\begin{Bmatrix} \mathbf{B_e} \\ 1 \end{Bmatrix} = \begin{Bmatrix} r\cos\sigma + L_c\cos(\sigma+\lambda) - (J_d+H)\sin(\sigma+\lambda) \\ r\sin\sigma + L_c\sin(\sigma+\lambda) + (J_d+H)\cos(\sigma+\lambda) \\ 1 \end{Bmatrix}$$
$$\equiv \begin{Bmatrix} q \\ |\mathbf{B_e} - \mathbf{U}| \\ 1 \end{Bmatrix} \quad (2)$$

where $Z(a)$ is a rotation of angle a about the Z-axis, $X(l)$ is a translation of distance l along the X-axis, σ is the angle between the adhesive and the corresponding wheg spoke, λ is the angle between the corresponding wheg spoke and the robot's chassis, U_d is the distance between the wheg's shaft and the corner $\mathbf{U}$ along the robot's chassis, e is the adhesive's thickness, and H is the height of the vertical tail.

Solving Eq. (1) and (2) gives the values of σ, λ and U_d for different q values, which gives the robot configuration as it contacts the second surface at variable distances from the intersecting corner $\mathbf{U}$. These robot configurations are useful for analyzing extensively the robot equilibrium at different instances that the robot contacts the second surface, as will be discussed in the next section.

B. External Transition Analysis

The free body diagram of the two-wheg climbing robot, as shown in Fig. 3(a), is used to analyze the success and failure conditions for robust external transitioning. The forces acting on the robot are the weight component of the robot (W) acting at the robot's center of gravity (CG), an equivalent normal force (F_{Rne}), shear force (F_{Rye}) and moment (M_{Re}) acting on the adhesive pivot P, and a normal reaction force (F_U) acting on the intersection between the robot's chassis and the corner $\mathbf{U}$ in the direction perpendicular to the chassis.

The system of equations for equilibrium during external transitioning is then obtained as

$$\sum F_x = 0 = F_U\sin\beta - W\sin\theta + F_{Rne} \quad (3)$$
$$\sum F_y = 0 = F_U\cos\beta - W\cos\theta - F_{Rye} \quad (4)$$
$$\sum M_P = 0 = F_U L_{yue}\sin\beta - W L_{ycge}\sin\theta - W L_{xcge}\cos\theta - M_{Re} \quad (5)$$

where θ is the slope angle of the first surface, $\beta = 270° - \sigma - \lambda$ is the acute angle between the direction of F_U and the second surface, L_{xcge} is the distance between the robot's CG and the second surface, and L_{ycge} and $L_{yue} = q$ are the distances of the the pivot P from the CG and the first surface respectively.

Similar to the analysis discussed in [20], there are two distinct cases of the force analysis: (I) when $F_U > 0$ and the chassis is in contact with the surface, and (II) when $F_U \leq 0$ and the chassis loses contact with the surface. Case II can happen, e.g., when the robot transits from a vertically-down to a horizontally-inverted orientation ($\theta = 270°$). In case I, the reaction force on the chassis provides the moment to counteract the weight component and there is no moment required on the adhesive ($M_{Re} = 0$). In case II, F_U needs to be set to zero as the chassis loses contact with the surface and the adhesive needs to provide the moment to counteract the weight component. In summary,

Case I Chassis is in contact with the surface ($F_U > 0$)

$$F_U = \frac{W}{q\sin\beta}(L_{ycge}\sin\theta + L_{xcge}\cos\theta)$$
$$M_{Re} = 0 \quad (6)$$

Case II Chassis loses contact with the surface ($F_U \leq 0$)

$$F_U = 0$$
$$M_{Re} = -W(L_{ycge}\sin\theta + L_{xcge}\cos\theta) \quad (7)$$

The forces acting on the adhesive can then be obtained as

$$F_{Rne} = W\sin\theta - F_U\sin\beta \quad (8)$$
$$F_{Rye} = F_U\cos\beta - W\cos\theta \quad (9)$$

Similar to [20], the motor torque requirement can be obtained by decoupling the free body diagram into the wheg and the chassis components. Then from the equilibrium equations, the motor torque requirement can be obtained as

$$T_{Se} = M_{Re} + F_{Rne}L_{yse} + F_{Rye}L_{xse} \quad (10)$$

where L_{yse} and L_{xse} are the perpendicular distances of the wheg's shaft from the first and second surface respectively.

C. Vertical Tail Analysis

The main difference between the previous versions and the current ORION-III is the novel vertical tail component, which is the key factor in accomplishing external transitions with only two whegs which has not been achieved in the past [12], [13], [17]. The theoretical ground behind the design decision can be derived from the force analysis discussed in the previous section.

Consider the robot without the vertical tail, i.e. $H = 0$ and $\beta = 0$, as shown in Fig. 3(b). This particular robot design actually creates another disctinct case of the force analysis where the forces acting on the robot is given by

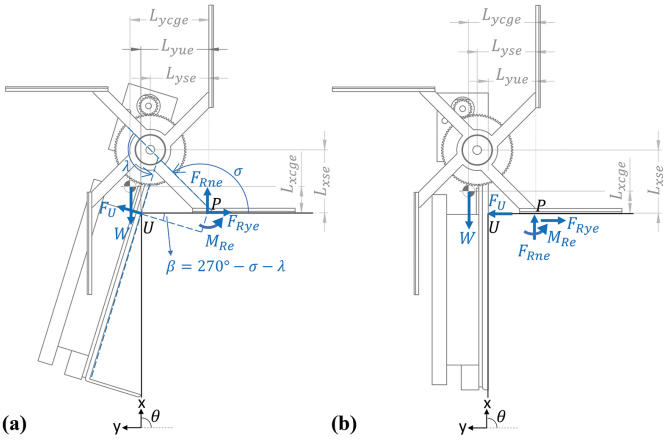

Fig. 3. Free body diagram of the robot during external transition, (a) with and (b) without the vertical tail component.

Case III Vertical tail component is absent ($\beta = 0$)

$$\begin{aligned} F_U &= \infty \\ M_{Re} &= -W(L_{ycge}\sin\theta + L_{xcge}\cos\theta) \\ F_{Rne} &= W\sin\theta \\ F_{Rye} &= F_U - W\cos\theta \end{aligned} \tag{11}$$

From Eq. (10), the motor torque requirement for case III can then be obtained as

$$T_{Se} = F_U L_{xse} - W\left[\sin\theta(L_{ycge} - L_{yse}) + \cos\theta(L_{xcge} + L_{xse})\right] \tag{12}$$

As can be seen from these derived equations, the reaction force on the chassis F_U is infinity for this particular case when the robot does not have the vertical tail component. This robot configuration is bound to fail because of either slip due to the high shear force on the adhesive or motor stall due to the high torque requirement, as there is F_U component in these two requirements. This occurence is observed and verified in the experiments, where the robot without vertical tail component is unable to perform the external transitions due to either slip or motor stall. Adding the simple vertical tail component results in $\beta > 0$, which breaks the robot from the case III failure and hence the success of the external transitions now depends on the fulfilment of the adhesive and motor torque requirements.

Based on this analysis, the vertical tail component is found to be a necessity and a design criteria for a two-wheg climbing robot to be able to perform external transitions. By changing the value of H in Eq. (2), the effect of the height of the vertical tail on the adhesive and motor torque requirements can also be analyzed.

D. Vertical Tail Modeling

To complete the climbing robot analysis, the additional vertical tail component needs to be incorporated into the flat-surface-climbing analysis in [20]. Fig. 4 shows the slider-crank model of the climbing robot (refer to [20]) (a) without and (b) with the vertical tail component. As shown in Fig. 4(b), as the vertical tail component is added, the robot will have a new $L_v(H)$ and $\alpha_v(H)$ values to replace the L and α values in the original analysis for the robot in Fig. 4(a).

To incorporate the additional component easily into the original analysis, the vertical tail is modeled as a separate mechanism as shown in Fig. 4(c). From the model, the following coordinate transformations relative to the origin frame at point **O** can be obtained:

$$\begin{aligned} \begin{Bmatrix} \mathbf{B_v} \\ 1 \end{Bmatrix} &= Z(\eta)X(L)Z(180^\circ - \mu)X(H)\begin{Bmatrix} 0 \\ 0 \\ 1 \end{Bmatrix} \\ &= \begin{Bmatrix} L\cos\eta - H\cos(\eta - \mu) \\ L\sin\eta - H\sin(\eta - \mu) \\ 1 \end{Bmatrix} \equiv \begin{Bmatrix} k \\ L_{ys} \\ 1 \end{Bmatrix} \end{aligned} \tag{13}$$

where $L_{ys} = \frac{r}{\sqrt{2}} - e$. Solving Eq. (13) gives the value of η for different H values, and the new L and α values for

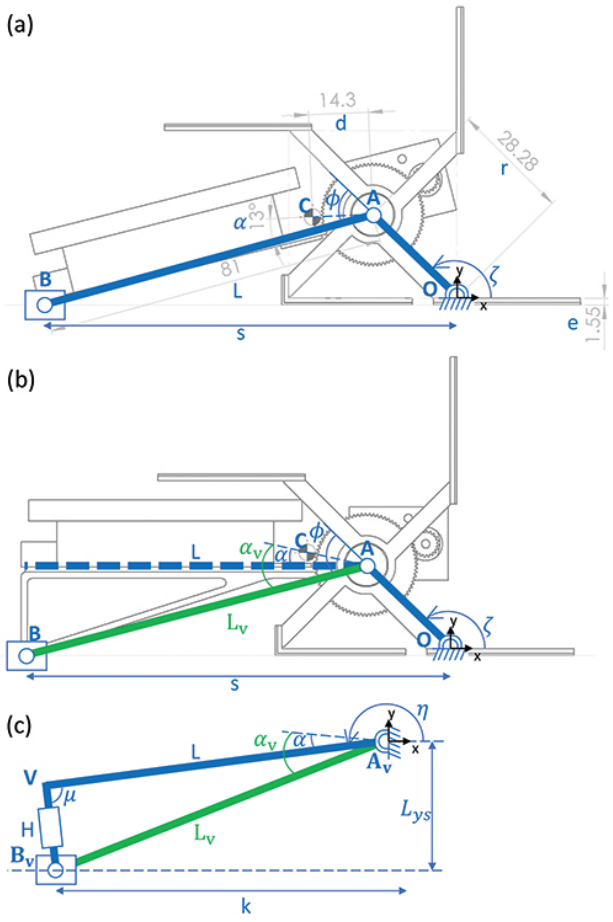

Fig. 4. Mechanism model of the climbing robot for the flat-surface-climbing analysis, (a) without and (b) with the vertical tail component, (c) separate mechanism model for the vertical tail component.

variable H values can be obtained as

$$L_v(H) = |\mathbf{B_v}| \tag{14}$$

$$\alpha_v(H) = \sin^{-1}\frac{H\sin\mu}{L_v(H)} + \alpha \tag{15}$$

Using these variable L_v and α_v values, the effect of the height of the vertical tail component on the adhesive and motor torque requirements for flat surface climbing can be easily incorporated and studied.

IV. RESULTS & EXPERIMENTS

In this section, the theoretical results in terms of the robot requirements and its expected perfomance based on the analysis are presented and discussed. Experiments were then conducted to verify the theoretical prediction.

A. Theoretical Results

In order to obtain the robot requirements and its expected performance for robust external transitioning, the analytical results are generated for all four cases of external transitions: vertical up to horizontal (VU $\rightarrow$ H, $\theta = 90^\circ$), horizontal to vertical down (H $\rightarrow$ VD, $\theta = 0^\circ$), vertical down to horizontal inverted (VD $\rightarrow$ HI, $\theta = 270^\circ$), and horizontal inverted to vertical up (HI $\rightarrow$ VU, $\theta = 180^\circ$), as depicted

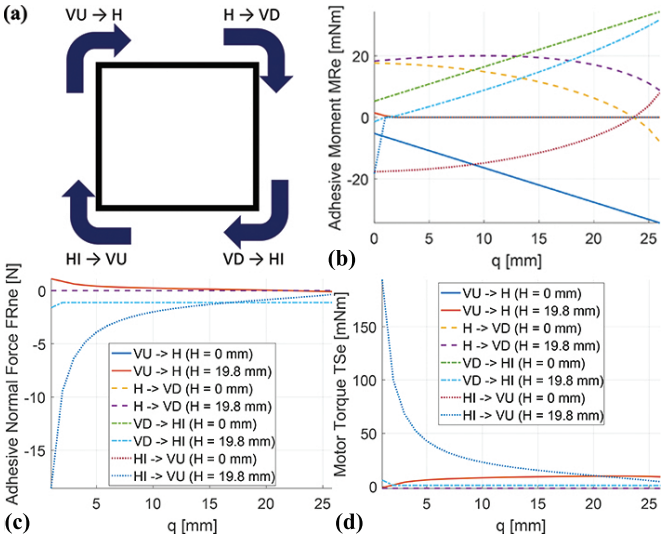

Fig. 5. (a) 4-way external transitions, (b) adhesive moment requirement, (c) adhesive normal force requirement, and (d) motor torque requirement for the transitions at various approach distances from the intersection corner.

in Fig. 5(a). As the adhesives generally have high shear adhesion strength, the results discussed will be in terms of the adhesive moment, normal adhesive force, and motor torque requirement, as plotted in Fig. 5(b), (c), and (d) respectively, for the different instances of approach distance q and the four different external transitions. As representatives and for clarity reason, only the plots for two different H values are generated: $H = 0$ mm i.e. robot without vertical tail and $H = L_{ys} = 19.8$ mm. Nevertheless, the results discussed here are generally applicable to any vertical tail H values, with difference only in the requirement values. For Fig. 5(c) and (d), only the results for the robot with the vertical tail can be seen as the robot without the vertical tail gives infinite values for the normal adhesive force and motor torque.

Inferred from Fig. 5(b), for a robot with a vertical tail height of 19.8 mm, the adhesive must be able to withstand a minimum moment of 35 mNm for complete robust external transitions at any instances of distance q. Interestingly, when looking at the results for the normal adhesive force (Fig. 5(c)) and required motor torque (Fig. 5(d)), as they can demand as high as 20 N force and 200 mNm torque respectively for the HI $\rightarrow$ VU transition at the instances of small q values, i.e. the robot's wheg contacts the second surface very near to the intersecting corner. This is because, as can be inferred from Eq. (6), F_U is inversely proportional to q, which then directly affects F_{Rne} (Eq. (8)) and T_{Se} (Eq. (10)). This effect is not prevalent for the H $\rightarrow$ VD and VD $\rightarrow$ HI transitions because they fall into case II where the chassis loses contact with the surface and $F_U = 0$. It also does not affect VU $\rightarrow$ H transition much because of the fact that at $\theta = 90°$, the robot dimension that affects F_U is L_{ycge} and it decreases as q decreases, which dampens the effect of small q. For the case of HI $\rightarrow$ VU, the robot dimension that affect F_U is L_{xcge}, which increases as q decreases and thus further magnifies F_U at small q.

Based on the analytical results, the climbing robot with the vertical tail is thus expected to have no difficulties performing VU $\rightarrow$ H, H $\rightarrow$ VD, and VD $\rightarrow$ HI transitions as long as the normal adhesive force, adhesive moment, and motor torque are above 2 N, 35 mNm, and 10 mNm respectively. However, it will have difficulty in performing HI $\rightarrow$ VU depending on the wheg approach distance from the intersecting corner due to the high normal adhesive force and motor torque requirements. This performance prediction based on the theoretical analysis is then verified through experiments on a physical prototype.

B. Experimental Results & Discussions

To maximize the possibility of HI $\rightarrow$ VU success, the maximum possible torque of 15 mNm provided by the motor will be used for the experimental tests. At this torque value, it was empirically found that the maximum adhesize dimension that the torque is able to peel off is 45 mm $\times$ 15 mm, which will be used for the experimental tests. Based on the flat-surface-climbing analysis ([20] & section III-D) and the adhesive characterization (section II-A), it was estimated that this dimension provides a normal adhesive force and adhesive moment of 3 N and 40 mNm respectively. With these specifications for the climbing robot, the prototype with the vertical tail height of 19.8 mm is expected to be able to robustly perform VU $\rightarrow$ H, H $\rightarrow$ VD, and VD $\rightarrow$ HI transitions while partially be able to perform HI $\rightarrow$ VU.

As predicted by the analysis, the robot without the vertical tail component was unable to perform the external transitions due to either adhesive slip or motor stall. Fig. 6(a)-(d) shows the photo snapshots of the climbing robot prototype with the vertical tail component performing the 4-way external transitions. As predicted by the analysis, the robot can perform VU $\rightarrow$ H (Fig. 6(a)) and H $\rightarrow$ VD (Fig. 6(b)) transitions robustly independent of the distance of the initial wheg contact with the second surface from the intersecting corner. For the HI $\rightarrow$ VU (Fig. 6(d)), the robot is only able to complete the transition if the wheg approaches the second surface far away from the intersection corner, as also predicted by the analysis.

The main discrepancy between the analytical and the experimental results is for the case of VD $\rightarrow$ HI (Fig. 6(c)). It was found that the robot has difficulty robustly performing this transition, where the robot would occasionally detach from the first surface before even contacting the second surface. The primary possible reason for this is due to the adhesive requirement for flat surface climbing, which was not considered yet in predicting the success and failure of the climbing robot.

Figure 7 shows the normal adhesive force and moment requirement for flat surface climbing at different slope angles using the analysis adapted from [20] and incorporating the additional vertical tail modeling in section III-D. As seen from the plot, climbing a slope of 270° (vertical down) requires as high as 39 mNm of adhesive moment. With the adhesive specifications used in the experiments, the robot might not have difficulty climbing vertically down if most

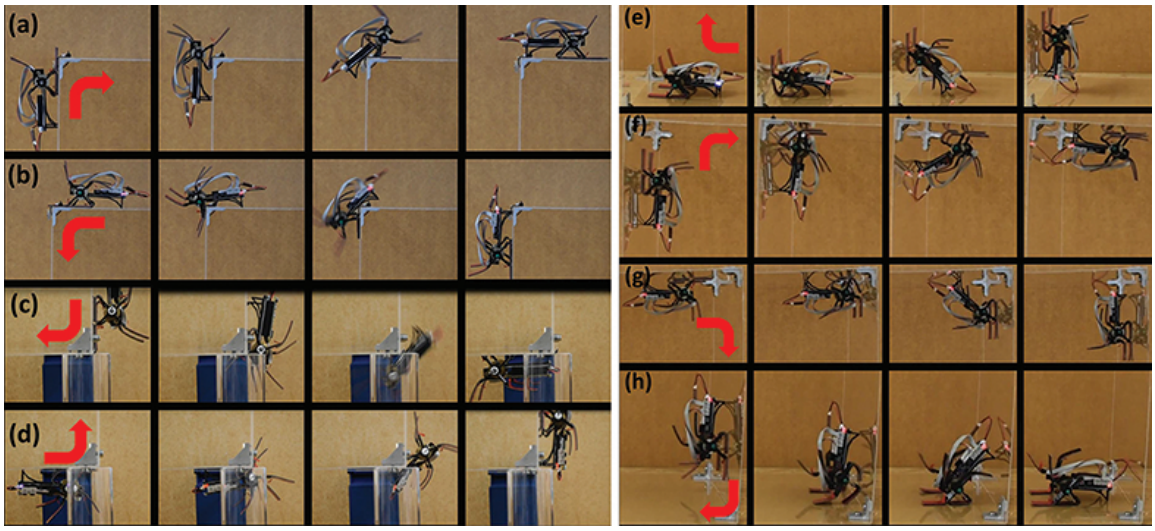

Fig. 6. Snapshots during external transitions, (a) vertical up to horizontal, (b) horizontal to vertical down, (c) vertical down to horizontal inverted, (d) horizontal inverted to vertical up; and internal transitions, (e) horizontal to vertical up, (f) vertical up to horizontal inverted, (g) horizontal inverted to vertical down, (h) vertical down to horizontal.

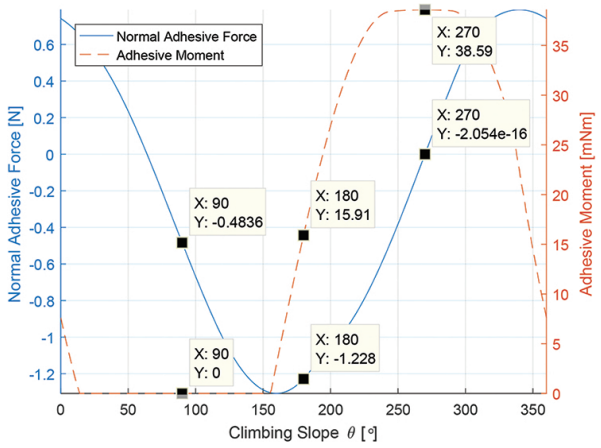

Fig. 7. Normal adhesive force and moment requirements for flat surface climbing at various slope angles for the robot with vertical tail component.

of the adhesive area is in contact with the surface. However during the transition, if the last wheg leaving the first surface is at a position very near to the intersecting corner, there is very little adhesive area that is in contact with the first surface to support the robot before the next wheg contacts the second surface. Thus, detachment may occur, which is what was observed in the experiments. The other external transitions are not affected by this because the normal adhesive forces and moments required for climbing horizontal, vertical up, and horizontal inverted are much lower than the capabilities of the adhesive used in the experiments.

As literature has shown that internal transitioning is easier to achieve, the climbing robot is also able to perform the 4-way internal transitions, as demonstrated in Fig. 6(e)-(h).

The performance of the climbing robot prototype that is developed in this work is mainly limited by the capabilities of the available adhesive and the motor. Should the motor and adhesive be able to meet the requirements obtained from the analysis, the climbing robot should be able to perform all the climbing and transitioning robustly. In the future, the robot dimensional optimization will be further studied based on the analysis results here to help to minimize the adhesive and the motor torque requirements and thus achieve a more robust two-wheg miniature climbing robot.

V. CONCLUSIONS

This paper presents the analysis, design, and development of a two-wheg miniature climbing robot capable of climbing any slope angles, 4-way internal transitions, and 4-way external transitions. The success and failure conditions to achieve the robust climbing and transitioning are discussed and analyzed extensively, resulting in a design basis for robust climbing and transitioning with a simple two-wheg climbing robot, which has not been able to be achieved in the past. The result of this study opens up the opportunity to miniaturize and develop a robust climbing robot requiring only two whegs, which was previously thought to be impossible. Based on the analysis, it was deduced that a passive vertical tail component is the key to achieving external transitions with a two-wheg climbing robot. A climbing robot prototype based on the design decision was developed and it was shown through experiments that the performance of the robot follows the theoretical analysis closely.

The outcome of the analysis can be used for robot design and dimensional optimization to minimize the adhesive and motor torque requirements, which will be part of the future works. Only the presence of a vertical tail component is studied and analyzed in this work. In the future, the shape of the tail that minimizes the adhesive and motor requirements can also be studied. The transition studied here is also only -90° convex angle. In the future, the analysis can be expanded into variable transition angles. Other future work also includes verifying further the analytical results through force and moment measurements on a custom-made system.

REFERENCES

[1] F. Tâche, W. Fischer, R. Siegwart, R. Moser, and F. Mondada, "Compact magnetic wheeled robot with high mobility for inspecting complex shaped pipe structures," in *Proc. IEEE/RSJ Int. Conf. Intell. Robots Syst.*, pp. 261-266, 2007.

[2] G. Lee, H. Kim, K. Seo, J. Kim, and H. S. Kim, "MultiTrack: A multi-linked track robot with suction adhesion for climbing and transition," *Robot. Auton. Syst.*, vol. 72, pp. 207-216, 2015.

[3] M. Malley, M. Rubenstein, and R. Nagpal, "Flippy: A soft, autonomous climber with simple sensing and control," in *Proc. IEEE/RSJ Int. Conf. Intell. Robots Syst.*, pp. 6533-6540, 2017.

[4] H. Prahlad, R. Pelrine, S. Stanford, J. Marlow, and R. Kornbluh, "Electroadhesive robotswall climbing robots enabled by a novel, robust, and electrically controllable adhesion technology," in *Proc. IEEE Int. Conf. Robot. Autom.*, pp. 3028-3033, 2008.

[5] R. Sahay, H. Y. Low, A. Baji, S. Foong, and K. L. Wood, "A State-of-the-Art Review and Analysis on the Design of Dry Adhesion Materials for Applications such as Climbing Micro-robots," *RSC Adv.*, vol. 5, no. 63, pp. 50821-50832, 2015.

[6] O. Unver, and M. Sitti, "Tankbot: A miniature, peeling based climber on rough and smooth surfaces," in *Proc. IEEE Int. Conf. Robot. Autom.*, pp. 2282-2287, 2009.

[7] O. Unver, and M. Sitti, "A miniature ceiling walking robot with flat tacky elastomeric footpads," in *Proc. IEEE Int. Conf. Robot. Autom.*, pp. 2276-2281, 2009.

[8] K. A. Daltorio, T. E. Wei, S. N. Gorb, R. E. Ritzmann, and R. D. Quinn, "Passive foot design and contact area analysis for climbing mini-whegs," in *Proc. IEEE Int. Conf. Robot. Autom.*, pp. 1274-1279, 2007.

[9] M. P. Murphy, W. Tso, M. Tanzini, and M. Sitti, "Waalbot: An agile small-scale wall climbing robot utilizing pressure sensitive adhesives," in *Proc. IEEE/RSJ Int. Conf. Intell. Robots Syst.*, pp. 3411-3416, 2006.

[10] K. A. Daltorio, A. D. Horchler, S. Gorb, R. E. Ritzmann, and R. D. Quinn, "A small wall-walking robot with compliant, adhesive feet," in *Proc. IEEE/RSJ Int. Conf. Intell. Robots Syst.*, pp. 3648-3653, 2005.

[11] S. Kim, M. Spenko, S. Trujillo, B. Heyneman, D. Santos, and M. R. Cutkosky, "Smooth vertical surface climbing with directional adhesion," *IEEE Trans. Robot.*, vol. 24, no. 1, pp. 65-74, 2008.

[12] M. P. Murphy, and M. Sitti, "Waalbot: An agile small-scale wall-climbing robot utilizing dry elastomer adhesives," *IEEE/ASME Trans. Mechatronics*, vol. 12, no. 3, pp. 330-338, 2007.

[13] W. A. Breckwoldt, K. A. Daltorio, L. Heepe, A. D. Horchler, S. N. Gorb, and R. D. Quinn, "Walking inverted on ceilings with wheel-legs and micro-structured adhesives," in *Proc. IEEE/RSJ Int. Conf. Intell. Robots Syst.*, pp. 3308-3313, 2015.

[14] O. Unver, and M. Sitti, "Tankbot: A palm-size, tank-like climbing robot using soft elastomer adhesive treads," *Int. J. Robot. Res.*, vol. 29, no. 14, pp. 1761-1777, 2010.

[15] T. Seo, and M. Sitti, "Tank-like module-based climbing robot using passive compliant joints," *IEEE/ASME Trans. Mechatronics*, vol. 18, no. 1, pp. 397-408, 2013.

[16] K. A. Daltorio, T. C. Witushynsky, G. D. Wile, L. R. Palmer, A. A. Malek, M. R. Ahmad, L. Southard, S.N. Gorb, R.E. Ritzmann, and R. D. Quinn, "A body joint improves vertical to horizontal transitions of a wall-climbing robot," in *Proc. IEEE Int. Conf. Robot. Autom.*, pp. 3046-3051, 2008.

[17] H. H. Hariri, D. C. Y. Koh, H. C. Lim, A. G. Dharmawan, V. D. Nguyen, G. S. Soh, S. Foong, R. Bouffanais, H. Y. Low, and K. L. Wood, "ORION-II: A Miniature Climbing Robot with Bilayer Compliant Tape for Autonomous Intelligent Surveillance and Reconnaissance," in *Proc. IEEE 15^{th} Int. Conf. Control Autom. Robot. Vis. (ICARCV)*, pp. 1621-1626, 2018.

[18] H. Shahsavan, and B. Zhao, "Bioinspired functionally graded adhesive materials: synergetic interplay of top viscouselastic layers with base micropillars," *Macromolecules*, vol. 47, no. 1, 353-364, 2013.

[19] A. G. Dharmawan, P. Xavier, H. H. Hariri, G. S. Soh, A. Baji, R. Bouffanais, S. Foong, H. Y. Lee, and K. L. Wood, "Design, Modeling and Experimentation of a Bio-Inspired Miniature Climbing Robot with Bilayer Dry Adhesives," *J. Mech. Robot*, in press, 2019.

[20] A. G. Dharmawan, P. Xavier, D. Anderson, K. B. Perez, H. H. Hariri, G. S. Soh, A. Baji, R. Bouffanais, S. Foong, H. Y. Lee, and K. L. Wood, "A Bio-Inspired Miniature Climbing Robot with Bilayer Dry Adhesives: Design, Modeling, and Experimentation," in *Proc. ASME Int. Des. Eng. Tech. Conf. Comput. Inform. Eng. Conf. (IDETC/CIE)*, pp. V05BT07A036, 2018.